Journal Pre-proof


# Propagation of waves in nonlocal-periodic systems

A.S. Rezaei , A. Carcaterra , S.V. Sorokin , A. Hvatov ,
F. Mezzani

PII: S0022-460X(21)00228-5
DOI: https://doi.org/10.1016/j.jsv.2021.116156
Reference: YJSVI 116156

To appear in: *Journal of Sound and Vibration*

Received date: 18 June 2020
Revised date: 25 March 2021
Accepted date: 19 April 2021

Please cite this article as: A.S. Rezaei , A. Carcaterra , S.V. Sorokin , A. Hvatov , F. Mezzani , Propagation of waves in nonlocal-periodic systems, *Journal of Sound and Vibration* (2021), doi: https://doi.org/10.1016/j.jsv.2021.116156

# Propagation of waves in nonlocal-periodic systems

A. S. Rezaei[a], A. Carcaterra[a], S. V. Sorokin[b], A. Hvatov[c], F. Mezzani[a]

[a]Department of Mechanical and Aerospace Engineering, Sapienza University of Rome, 00184, Rome, Italy

[b]Department of Mechanical and Manufacturing Engineering, Aalborg University, Fibigerstrade 16, 9220, Aalborg, Denmark

[c]National Centre for Cognitive Research, ITMO University, 197101, 49 Kronverksky pr., St. Petersburg, Russia

[*]Corresponding author. amirsajjad.rezaei@uniroma1.it

**Abstract**

This paper is concerned with emergence of novel effects in wave propagation in one-dimensional waveguides, when integrated with periodic nonlocalities. The nonlocalities are introduced by a connectivity superimposed to a conventional waveguide and depicted as a graph with trees and leaves, each with its own periodicity. Merging nonlocality and periodicity notions induces a distinction between homogenous and non-homogenous periodic configurations. Specifically, various unconventional phenomena linked to the presence of nonlocalities result in disruption of the energy transmission in such systems, disclosing new opportunities for vibration isolation applications. To demonstrate these effects, simple models of propagation of plane extension/compression waves in a uniform infinite rod equipped with co-axial spring-like elements is used. The homogenous case is analysed by a direct double, space and time, Fourier transform, leading to discussion of unusual dispersion effects, including vanishing and negative group velocity. In the non-homogeneous case, the canonical Floquet theory is used to identify stopbands and control their positions in the frequency domain. The results are compared with eigenfrequency analysis of unit periodicity cells and finite structures. Next, the forcing problem is considered and the insertion losses in a semi-infinite rod with nonlocal spring effects are computed to corroborate predictions of Floquet theory, providing physical explanations of the obtained results. Finally, possibilities to employ the non-local interaction forces in an active control format to generate stopbands at arbitrarily low frequencies are highlighted.

Keywords

Periodic structures, Wave propagation, Long-range interactions, Floquet theory, Eigenfrequency analysis, Insertion losses, Graph theory

## 1. Introduction

The major rationale for conducting research on periodic configurations is the design of structures which provide broad stopbands especially in the low frequency range. In fact, Brillouin [1] indicated that periodic structures are capable of offering gaps in their band structure. Typically, such structures are remarkably demanding in terms of isolation technologies and transducer design; and the optimal design of these applications is contingent

upon low frequency band gaps. Various types of periodic structures are proposed by researchers to reach that end.

A rich point of view on metamaterials is recently proposed, in which exclusive first neighbour interaction is challenged, allowing for nonlocal actions at a fixed or unlimited window. Under such circumstances, the nature of the system is deeply influenced, enabling the manipulation of travelling waves by properly tailoring the topology and the intensity of the interaction between distant points. Various means for distant interaction include magnetic inclusions and external spring-like elements, which can cause instant energy transmission across the system.

Studies in nonlocal continuum mechanics revealed how introduction of long-range interactions may cause some strange wave propagation behaviours dissimilar to the corresponding response of conventional elastic solids [2,3]. For instance, Eringen's nonlocal theory of elasticity [3–5] modifies the constitutive relation of a medium (with respect to the classical theory of elasticity) by considering an addition convolution terms, which describes the dependence of the state of stress on the deformation at the point along with the that of all other point within the domain, and subsequently the effect of this revision on the status of travelling wave in the corresponding media. Among other nonlocal formulations in continuum mechanics, Silling [6] introduced an integro-differential formalism called "Peridynamics", which helps to avoid singularities in domain with discontinuity by considering a confined interaction region in the vicinity of each point. Peridynamics does not involve the strain and stress explicitly by an integral term in terms of deformation components unlike classical theory of elasticity and Eringen's nonlocal theory.

In the context of long-range systems, several contributions have been published in past few decades [7–11]. For instance, Kunin [12] provided the context for studying of one-dimensional elastic media with microstructure such as ionic and non-ionic crystals. Several lattice models have been considered in his work, which take into account the effect of action in the distance between the non-adjacent points of such domains by means of simple elastic connectors (spring). Zingales [13] presented a model to investigate the wave propagation in finite one-dimensional mechanically based nonlocal elastic solids, showing correlations between this type of solids and the well-known Kroner-Eringen integral model. The discrete model presented Carpentieri et al. [14], which shares resemblance with that of Zingales [15] assumes a modified version for the stress-strain relation equipped with a particular attenuation function, which causes fractional derivatives to appear in the associated dynamics. To identify the existing propagation regimes in one-dimensional long-range systems, Carcaterra and co-authors [16–21] confirmed the existence of some unusual regimes such as negative and hypersonic group velocity, providing a general mapping of these effects, even in the presence of delay in nonlocal propagation. In the light of these points, introduction of nonlocalities seems promising to improve the design of acoustic metamaterials.

A review of analyses for identifying the state of waves travelling through conventional continuous periodic structures, including beams, plates and cylindrical shells, is provided in the classical work by Mead [22]. Phononic crystals (PCs) are usually defined as artificial materials made of periodic arrangement of scatterers embedded in a matrix [23], and they

have been in the centre of attention for the past three decades [24–27]. However, large size phononic crystals are required to absorb real-life sound waves since they must be arranged spatially on the order of the matrix acoustic wavelength [28]. To overcome the limits of PCs, the acoustic metamaterials, which are composed of mechanical subunits embedded within thin-walled elements, are employed. In the literature, the effect of both geometrical parameters for placement of resonators in arrays, as well as the type of the resonator itself, on the wave transmission has been investigated comprehensively [29–31]. The possibility of designing materials with negative effective mechanical properties was then investigated and observed experimentally [32–34]. On the other hand, Floquet's principle can be employed as a powerful tool to highlight the stopband formation mechanism in the band structure of various configurations such as periodic elastic compound rods (PECR), periodically corrugated elastic layers [35–37]. In a separate study, Hvatov and Sorokin [38] compared the eigenfrequency spectra of some finite compound structures with the results obtained from the plane wave analysis of their infinite counterpart and investigated the effect of the number of unit-cells on the spectrum.

Certainly, the fundamental studies of Eringen [5] and Kunin [12] inspired the authors to attack the objective (manipulation of wave path) by introducing nonlocalities to systems. Along this line, adopting mathematical tools, which provide the possibility of defining particular interaction regions for each part of the systems, similar to Peridynamics approach [6], seem to be an efficient choice.

However, to the best of authors' knowledge, so far, no wave analysis is performed for combining the effects of periodicity and nonlocality on the performance of acoustic metamaterials; this represents the novel contribution of the present work.

Moreover, novel is the study of the systematic topology of the long-range connectivity, represented through a graph structure with a double characteristic periodicity, of the trees and the leaves, respectively, leading to distinguish between homogenous and non-homogenous distribution of nonlocalities. The first type is described by an equation of motion with constant coefficients but with periodically spatial-delayed terms. The second type is characterised by an equation of motion with periodic coefficients.

The effects of both types of systems are studied using the simple model of propagation of plane dilatation/compression waves in an otherwise uniform rod. First, several cases of the long-range homogenous periodic and long-range homogenous structure, where the distribution of nonlocalities are the same for each point of the system, are considered, and the corresponding propagation effects are captured by a direct double Fourier transform and the study of the associated dispersion relationship. Analytical results are feasible because of the type of considered long-range connectors, disclosing the most important wave propagation effects of both the long-range connectivity and related (leaf-) periodicity. Next, the case of non-homogeneous periodicity is studied, then the periodic positioning of nonlocalities on repeating rod elements generates a conventional periodic configuration. The working mechanism of these nonlocalities is further inspected by examining energy flux and insertion losses in a semi-infinite waveguide, which includes a "periodic insert" of the same nature. Note that all anomalies reported throughout the paper are indeed concerned with disruption of the energy transmission in the systems under studying.

The paper is structured as follows. In section 2, a formal distinction between nonlocal homogenous and non-homogeneous periodicity is introduced following the introduction of the graph-periodicity concept. In section 3, the concepts of nonlocal interactions and long-range forces of the first type are illustrated in four examples of progressive complexity and the arising phenomena have been underlined. The analysis suggests the possibility of achieving wave-stopping at particular frequencies as well as backward energy transmission in certain frequency ranges. In section 4, a mathematical formulation for the second type of long-range periodicity is presented, where the periodicity is induced by nonlocalities embedded in a conventional waveguide. The results given in this section demonstrate the generation of stopbands, without the conventional impedance mismatch, and purely related to the long-range periodicity. Section 5 addresses the possibility of pulling the gaps to the very low frequencies by redesigning the system through active control elements. A detailed analysis of insertion losses in the semi-infinite rod containing a specific number of periodic cells, described in the previous sections, is provided in section 6. An important 'nonlocality-induced' phenomenon is highlighted in section 7, where the interaction between the spring-born force and that carried along the segments is studied. Finally, the concluding remarks are given in section 8.

## 2. Long-range graph-periodicity: non-homogenous and homogenous cases

Notions of long-range interactions and periodicity, when suitably combined, lead to an interesting distinction between two different ways of building up long-range connectivity templates, enriching both the scenarios of nonlocal elasticity and periodic systems. This distinction is important for the present investigation, enlightening a physical difference together with the related different mathematical approaches to the corresponding problems.

A classical periodic system shows, in general, a modular structure, where the characteristic module sequentially replicates itself along the system. This produces, as a mathematical counterpart, a differential equation of motion with periodic coefficients that characterize a conventional and genuine periodicity. We show ahead that a wider scenario discloses through the concept of graph-periodicity leading to some forms of periodicity even in the presence of constant coefficients.

The focus is on a conventional infinite waveguide, described for simplicity by the standard wave equation $EA\frac{\partial^2 u}{\partial x^2} - \rho A\frac{\partial^2 u}{\partial t^2}$, with $u(x,t)$, $\rho$, $E$ and $A$ being the longitudinal displacement, mass density, Young's modulus, and the cross-section area, respectively. An additional archetypal long-range connectivity is superimposed, connecting, by a suitable long-range set of connectors, i.e. equivalent springs and in different possible fashions, distant points of the host waveguide. Note that in the models provided in the following sections (based on this concept), the nonlocalities are modelled by simple mechanical component (elastic links), which are similar to those presented in Ref. [12,14,15].

For a given superimposed connectivity $G$ on a conventional waveguide, we can introduce its formal description through the symbol $G_T\left(x_{-N}, x_{-N+1,} \dots, x_{-1}, x_T, x_{1,} x_{2,} \dots, x_M\right)$. The graph $G_T$ specifies the set of connectors applied to the waveguide. Namely, the graph has a *tree* at

$x_T$ connected to each of the selected points $x_{1,}x_{2,} \dots, x_M$ on its right, and to each of the points $x_{-N}, x_{-N+1,} \dots, x_{-1}$ on its left, that are the *leaves* of $G_T$. $M$ and $N$ are generally different, and the end points of leaves not necessarily equally spaced. In case the leaves are equally spaced, the spacing $L$ is named the *period of the leaves* and the related connectivity *leaf-periodic* (see Fig. 1).

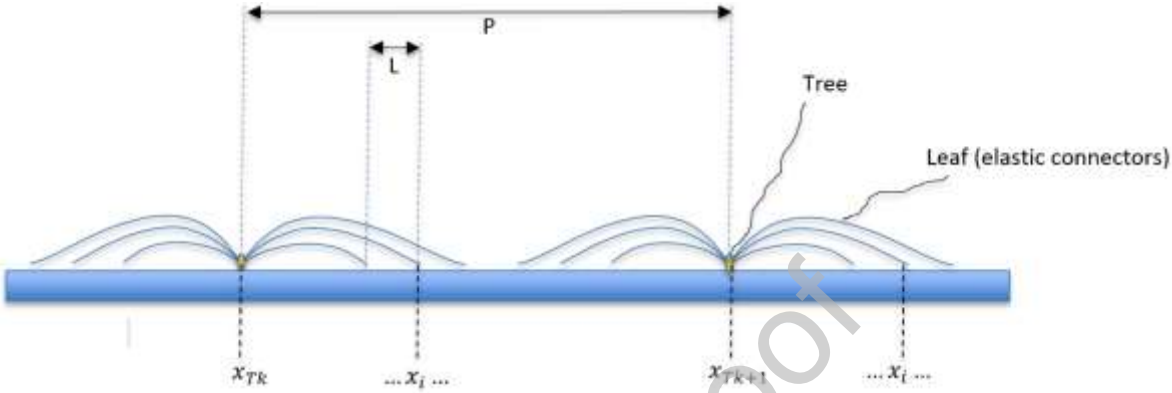


**Fig. 1**: Sketch illustrating the graph-periodicity concept

The superposition of more connectivity graphs $G_{Tk}$ with different trees positions $x_{Tk}$, for $k = 1,2 \dots, M_P$, generates a new long-range connectivity graph $G$:

$$G = \cup_{k=1}^{M_P} G_{Tk} \tag{1}$$

If the trees are equally spaced, the spacing $P$ is the *period of the trees*, distinct from the period of the leaves $L$ and the connectivity is *tree-periodic* (in some cases $P = L$).

The combination of tree-periodicity and leaf-periodicity leads to discuss several interesting cases, some of them considered in the present paper.

A connectivity $G$ that is tree-periodic (independently of the leaf periodicity) produces a structure that is periodic in a genuine-conventional sense, i.e. its equation of motion has periodic coefficients. In fact, the connectivity $G$ applies only to specifically selected points along the waveguide, and we call for this reason the structure *long-range non-homogenous periodic* and its connectivity $G_{n-hom}$, a case analysed in this paper.

If the connectivity is tree-periodic and leaf-periodic, we can generate a *long-range homogeneous periodic* structure through $G_{hom} = \lim_{P \to 0} G_{n-hom}$, that has a continuous distribution of trees. In fact, this means that the same connectivity applies identically to any point at $x$ (the trees becoming infinitely dense), therefore producing homogeneity, and the presence of constant coefficients in the equation of motion (not periodic anymore). However, although in this way the tree-periodicity disappears, the leaf-periodicity still holds. Therefore, we have a constant coefficients equation of motion, but still characterized by a residual leaf-periodicity, that is an intriguing new concept investigated in the present paper.

If the leaves are non-periodic, $G_{hom} = \lim_{P \to 0} T_{n-hom}$ produces simply a *long-range homogenous* connectivity without elements of periodicity, that is another case investigated in the present paper. Here $T_{n-hom}$ refers to the tree in a non-homogenous configuration.

The case $G_{hom} = \lim_{P \to 0, L \to 0} T_{n-hom}$ produce finally a continuous distribution of trees and leaves, periodicity is absent, and again a simply a *long-range homogenous* connectivity is defined, also analysed in the present paper.

Let us illustrate, by elemental examples, the equations of motion related to the previously introduced graph-periodicity.

The modified waveguide equation, when including the presence of the long-range elastic links, becomes:

$$EA\frac{\partial^2 u}{\partial x^2} - \rho A\frac{\partial^2 u}{\partial t^2} + \Gamma(x,t) = 0 \qquad (2)$$

Let us consider, as a first example, a periodic-tree and periodic-leaf connectivity, with an infinite number of trees along the waveguide, each with $N$ leaves. The single-tree connectivity $G_T$, with its tree at $x_T$, is associated to the operator $\Gamma_T(x,t) = -\chi\sum_{i=-N}^{+N}\delta(x - x_T)[u(x,t) - u(x - iL,t)]$ with $\chi$ being the stiffness of elastic connectors (see Fig. 1). Simple consideration, including serially repeated trees, shows the long-range term $\Gamma_{n-hom}(x,t)$ reads:

$$\Gamma_{n-hom}(x,t) = -\chi\sum_{r=-\infty}^{+\infty}\sum_{i=-N}^{+N}\delta(x - rP)[u(x,t) - u(x - iL,t)] \qquad (3)$$

The nature of the equation $EA\frac{\partial^2 u}{\partial x^2} - \rho A\frac{\partial^2 u}{\partial t^2} + \Gamma_{n-hom}(x,t) = 0$ is differential, with periodic coefficients: the differential part is $EA\frac{\partial^2 u}{\partial x^2} - \rho A\frac{\partial^2 u}{\partial t^2}$, the periodic coefficients are $\chi\delta(x - rP)$, and:

$$\Gamma(x,t) = \Gamma(x + nP,t), \quad \forall n \in N \qquad (4)$$

This is an example of *long-range non-homogenous periodicity*. The most acknowledged method for periodic coefficients equations is the Floquet theorem.

However, as seen through the graph-periodicity concept, one can conceive a different way of using the same connectivity template that is not selective, i.e. does not involve only special points along the waveguide (as those at $x_{Tr} = rP$ as in the previous case) but it applies serially and homogenously to each point $x$ of the structure (that means $P$ becomes infinitely small). Hence, the name *long-range homogeneous periodicity*. In this case, the equation of motion does not exhibit periodic coefficients anymore. In fact:

$$\Gamma_{hom}(x,t) = -\chi\sum_{i=-N}^{N}[u(x,t) - u(x - iL,t)] \qquad (5)$$

This operator shows a different nature with respect to the form (3) previously presented. Using the form (5), Eq. (2) becomes a differential-delay equation with constant coefficients, i.e. $EA\frac{\partial^2 u}{\partial x^2} - \rho A\frac{\partial^2 u}{\partial t^2} - \chi\sum_{i=-N}^{N} u(x,t) - u(x - iL,t) = 0$. Although a periodically delayed

term appears as $\sum_{i=-N}^{N} u(x-iL,t)$, the coefficients are constant. In this case the Floquet theorem, the typical tool for genuine periodic structures, can be skipped and replaced by a simpler direct double Fourier transform of the equation of motion. Note that in the models provided in the following sections (based on this concept), the nonlocalities are modelled by simple mechanical component (elastic links), which are similar to those presented in Ref. [14,15].

More precisely, the first tree-periodicity case requires, because of the non-homogenous nature of the structure, a piecewise solution, each part living within any module of the system, i.e.:

$$u^{(i)}(x,t) = \left(A^{(i)}e^{jkx} + A^{(i)*}e^{-jkx}\right)e^{j\omega t}, \;\; x \in [x_i, x_i + P] \tag{6}$$

Different solutions satisfy continuity conditions at the module's boundaries, i.e. at $x_i \; and \; x_i + P$, and the Floquet's theory finds the non-trivial solutions for the unknown coefficients $A^{(i)}$. A set of eigenvalues follows for the wavenumbers, and their nature establishes the chance of propagating waves or inhibiting them (stopband effects).

The second case, with homogenous nature, due to the constant coefficients, permits a direct double Fourier transform, space and time, with a continuous solution along the entire waveguide (no need to express a piecewise solution as for periodic coefficients):

$$u(x,t) = \int_{-\infty}^{+\infty}\int_{-\infty}^{+\infty} W(k,\omega)\, e^{jkx} e^{j\omega t} dk\, d\omega \tag{7}$$

Its substitution into the equation of motion produces the dispersion relationship $k(\omega)$ and its nature determines the chance of wave propagation or its inhibition, and additionally the group velocity behaviour of the waveguide is determined.

Although the two methods do not admit any mathematical interchange, and each type needs its own technique, on the physical ground, the interpretation of the results of the two methods are comparable. In fact, they both rely of the nature of the complex wavenumber (whatever its mathematical origin, i.e. the eigenvalues analysis or the dispersion relationship), as an indicator of the kind of waves established along the waveguide.

For both the different kinds of periodicity, some transition effects are expected when the wavelength $\lambda$ becomes much smaller than $P$, and/or of $L$ i.e. $kP >> 1$, and/or $kL >> 1$ where the wave energy remains trapped into the periodic inclusions, conferring to the system properties of energy propagation disruption in some frequency range.

To synthesize, different types of long-range configuration discussed above as well as their associated characteristics are collected into Table 1.

**Table 1:** Different types of long-range configurations based on graph-periodicity concept

| Type | Characteristics | Equation property | Solution method |
|---|---|---|---|
| non-homogenous periodic/ tree-periodic | Constant $P$ | Differential equation with periodic coefficients | Floquet theorem |
| homogenous periodic/ | $P \to 0$ & | Differential equation | Spatiotemporal Fourier |

| | | | |
|---|---|---|---|
| leaf periodic | Constant $L$ | with constant coefficients | transform |
| homogenous | $P \to 0$ & variable $L$ or L→ 0 | Differential and integral-differential equations with constant coefficients | Spatiotemporal Fourier transform |

In both cases, namely homogenous and non-homogenous periodicity, peculiar wave propagation effects emerge that include band gaps, wave stopping, negative group velocity and instabilities that amount to a rather rich scenario investigated in detail in the next sections.

Under the physical point of view, one can include the long-range nonlocalities in two different ways. The first uses solid elastic connectors, linking different sections of the conventional waveguide. This kind of connectivity leads to genuine periodic structures. An example of realization of this kind of connectivity is shown in Fig. 2. The internal core is the conventional waveguide, and an external shell supports the superimposed elastic links. The external shell connects to the core through a set of bulkheads (the flexural deformation and mass of which is negligible). Longitudinal traction and compression forces of the shell load the internal waveguide through the bulkheads (inertia effects of the shell are negligible in comparison with those of the core-waveguide). This structure, for example, can implement the configurations investigated in Fig. 12 and Fig. 17, that are cases of tree-periodic systems. However, these cases show a connection only between pairs of sections of the conventional waveguide. In fact, more general cases of long-range connectivity, in which each section of the conventional waveguide connects to a large (or potentially infinite) number of other sections, as for the cases investigated in Fig. 4 and Fig. 9, is difficult to implement by solid elastic connectors. In such cases, use of magnets inserted into the conventional waveguide, permits long-range magnetic interactions, including coupling forces among all the sections, where the magnets are located. This arrangement is represented in Fig. 3.

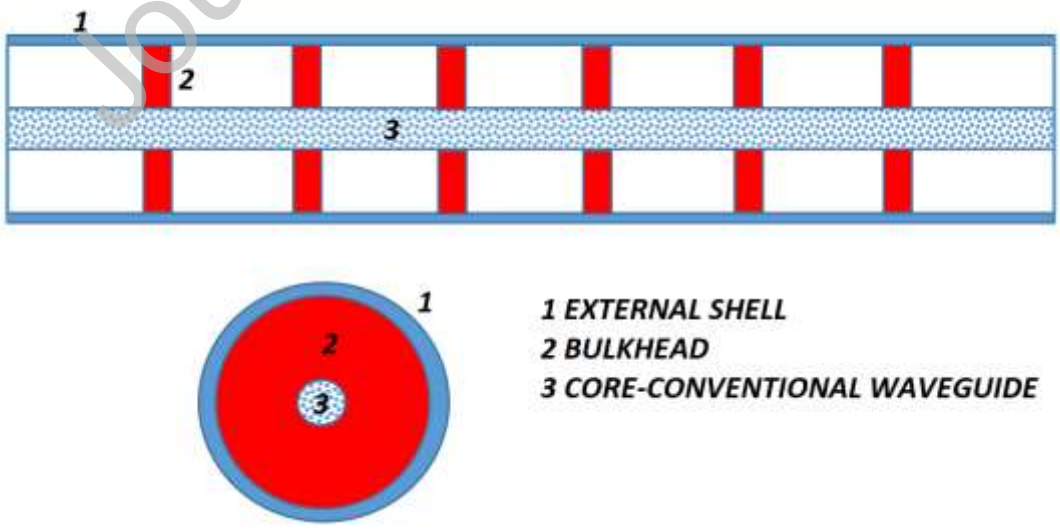


**Fig. 2:** A mechanical model for realization of a long-range tree-periodic structure

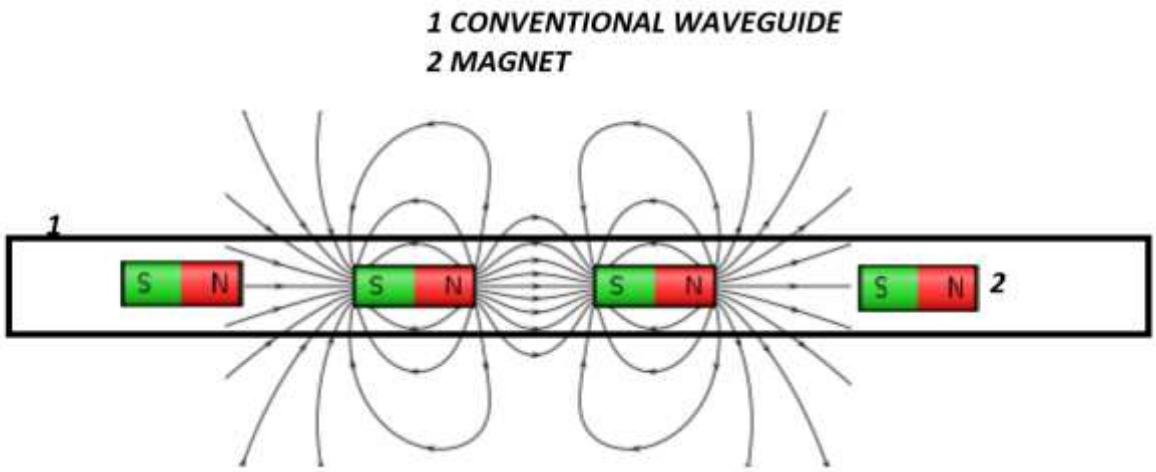


**Fig. 3:** A mechanical model for realization of a long-range leaf-periodic structure

## 3. Nonlocal homogenous periodic waveguides

In this section, effects of classical nonlocalities in propagation of the plane wave of axial deformation in a rod are discussed. Several arrangements of long-range operators acting as spring-like links are considered. In each case, the instantaneously transmitted force is proportional to the difference between the displacements of the ends of a link.

With reference to the graph-periodic concept introduced in the previous section, in section 3.1 we analyse the case of long-range homogenous-periodic structure, characterized by a periodicity of the leaves, while the periodicity of the trees is lost because they continuously distribute ($P$ tends to zero). Two examples consider both constant and variable stiffness of the connectors.

In section 3.2, the leaf-periodicity is lost making leaves non-equally spaced or continuously distributed. In those cases, we have simply a long-range homogenous structure.

### 3.1. Open interaction region

To begin with, a very simple case is considered. The behaviour of a homogenous-periodic waveguide with long-range interaction is presented, where the leaves are not confined to the tree vicinity, but they extend arbitrarily far, ideally even at infinite distance. The leaf-period is $L$, while the tree-periodicity disappears, since $P$ tends to zero.

The long-range forces are produced by springs of the same stiffness $\chi$, which connect any point $x$ to its counterparts located at the distances $iL$, as shown in Fig. 4. Here, $L$ is an arbitrary length and $i$ being an integer multiplier.

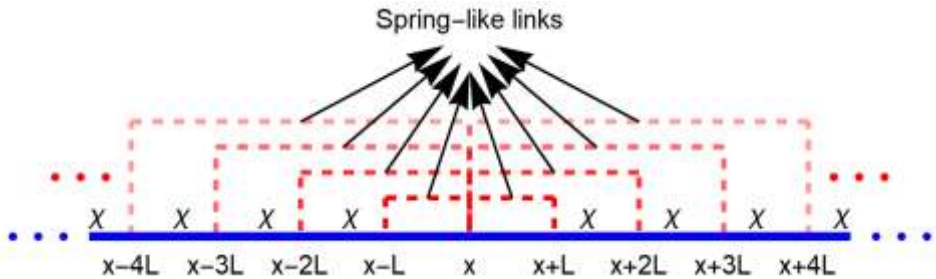

**Fig. 4:** Homogeneous-periodic waveguide with equally spaced nonlocalities

The resulting equation of motion is:

$$\rho A \frac{\partial^2 u(x,t)}{\partial t^2} = EA \frac{\partial^2 u(x,t)}{\partial x^2} - \chi \sum_{i=-N}^{N} [u(x,t) - u(x+iL,t)] \quad (8)$$

and $N$ is an arbitrary integer number.

Standard space-time Fourier transform of Eq. (8), yields the dispersion relation, which is written in the nondimensional form as:

$$K^2 - \Omega^2 + \widehat{K} \sum_{i=-N}^{N} \left[1 - e^{jiK}\right] = 0 \quad (9)$$

Here, $K = kL$ and $\Omega = \omega L \sqrt{\rho/E}$ are the nondimensional wavenumber and the nondimensional frequency, in the order given. $\mathrm{Z} = \chi L^2/EA$ is a nondimensional parameter, which scales the stiffness of the springs, and, therefore, intensity of long-range forces, to the stiffness of a rod. To highlight the nonlocality-induced phenomena in the response of the system, phase velocity $c_\phi = \Omega/K$ and group velocity $c_g = d\Omega/dK$ against the nondimensional wavenumber $K$ are displayed in Fig. 5 and Fig. 6, respectively.

Based on Fig. 5, by integrating the conventional waveguide with spring-like links, the corresponding value for phase velocity associated with travelling waves of very long wavelength ($K \to 0$) is rather high though the velocity drops sharply as $K$ increases, and eventually tends to unity at $K = 2\pi$ (D'Alembert waveguide's response). This implies that introduction of spring-like links influences the phase velocity response substantially in the low wavenumber band. Besides, systems with larger $N$ provide higher values of $c_\phi$, when the wavenumber tends to zero.

Regarding the group velocity response, considerable fluctuations in the speed of wave envelope with respect to that of the D'Alembert waveguide (marked in red) are observed in Fig. 6. The curves reveal the possibility of achieving wave-stopping and negative group velocity. Wave-stopping, i.e. zero group velocity, implies that the energy is forced to stop travelling across the domain at certain wavenumbers/frequencies. Furthermore, the model allows for backward moving energy propagation within the certain wavenumber/frequency bands with the extremes determined by the wave-stopping wavenumbers/frequencies.

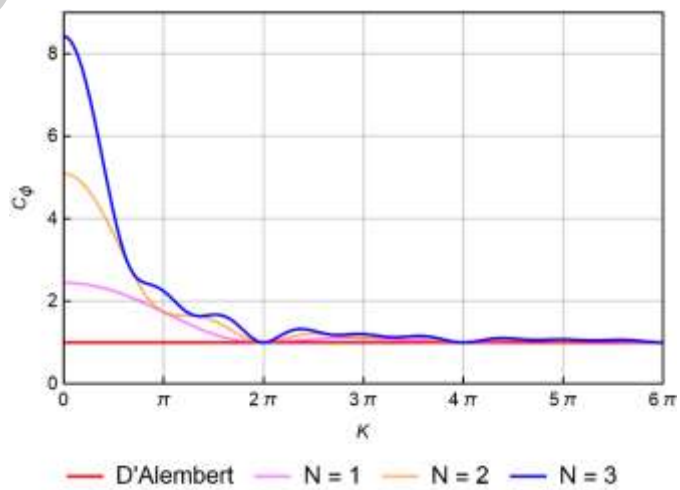

**Fig. 5:** Phase velocity curves for the homogenous periodic waveguide with equally spaced nonlocalities of same stiffness (Z = 5)

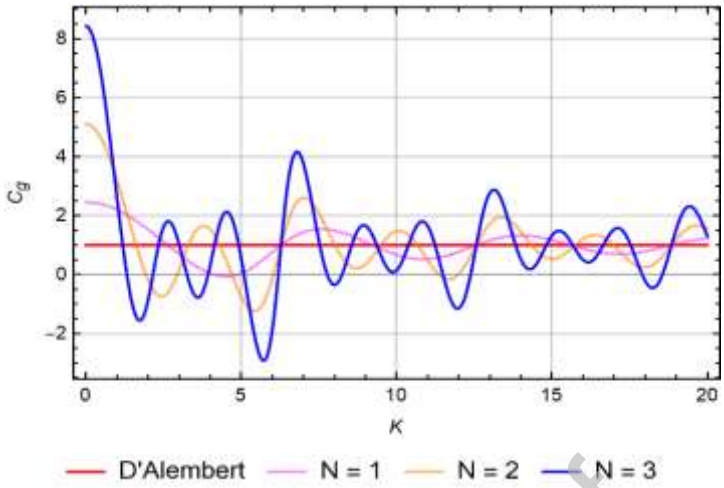


**Fig. 6:** Group velocity curves for the homogenous periodic waveguide with equally spaced nonlocalities of same stiffness (Z = 5)

Looking at Fig. 6, it appears that wave-stopping and negative group velocity emerge only if the value of the Z is above a critical value, $Z > Z_{cr}$, where $Z_{cr}$ depends on $N$. This point is clearly demonstrated in Fig. 7, where the variation of group velocity plotted for systems characterised by different value of Z ($N = 5$). Based on the figure, the amplitude of peaks increases as Z rises, providing the possibility of achieving more wavenumber bandwidth within which the group velocity turns negative. For instance, only two bandwidths with such feature are evident for a waveguide with $Z = 1$ in the plotted range while a system with $Z = 5$ yields fourteen similar bandwidths. In fact, the peaks become more pronounced for any super critical value of Z ($Z_{cr} = 0.2022$), leading to higher number of bandwidths with such characteristics (zero/negative group velocity).

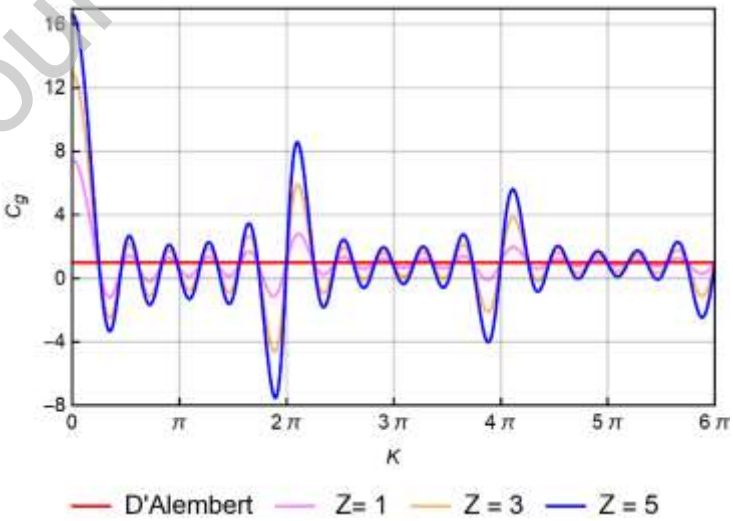


**Fig. 7:** Group velocity curves for the homogenous periodic waveguide with equally spaced nonlocalities of different stiffness (N = 5)

Note that Eq. (9), is meaningful only for a finite $N$. In fact, $\lim_{N \to \infty} \sum_{i=-N}^{N} [1 - e^{jiK}] = \infty$. However, if we introduce a variable stiffness decreasing with $i$, for example $Z/2^{|i|}$, the dispersion relation takes the form:

$$K^2 - \Omega^2 + Z \sum_{i=-N}^{N} \frac{[1-e^{jiK}]}{2^{|i|}} = 0 \tag{10}$$

The assumption regarding the stiffness of elastic connectors (monotonically decreasing by distance) corresponds to physical systems since usually the intensity long-range forces is proportionally stronger when the non-adjacent parts of a system are closer to one another.
As $N$ tends to infinity, the above equation reduces to the following simple form:

$$K^2 - \Omega^2 + 3Z\left(1 - \frac{1}{5 - 4\cos K}\right) = 0 \tag{11}$$

with the corresponding group velocity in a closed form:

$$C_g = \frac{6Z\sin(K) + 33K + 8K\left(\cos(2K) - 5\cos(K)\right)}{(4\cos(K) - 5)^{\frac{3}{2}} \sqrt{4\cos(K)(K^2 + 3Z) - 5K^2 - 12Z}} \tag{12}$$

characterized by the nondimensional parameter Z. For $N \to \infty$, the group velocity (12) is plotted in Fig. 8, together with the cases for $N = 1, 5, 10$. Note how the group velocity rapidly converges to the case $N \to \infty$, for which, $Z_{cr} \sim 4.353$.

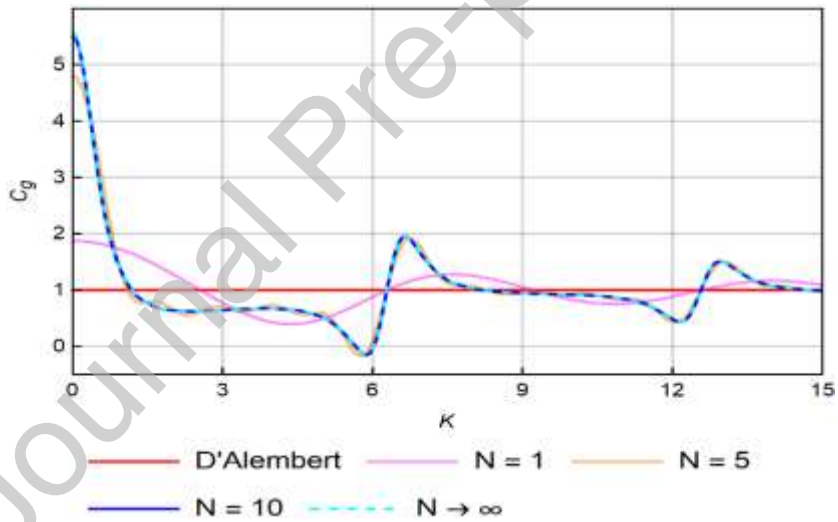


**Fig. 8:** Group velocity curves for the homogenous periodic waveguide with equally spaced nonlocalities of different stiffness ($Z = 5$)

### 3.2. Confined interaction region

In this example, a system in which the connection points (ends points of the leaves) are not equally spaced is considered, and the distance between two consecutive connectors is $x_{i+1} - x_i = L/2^{|i|}$. This means both the tree-periodicity and the leaf-periodicity are lost, and the investigated system is simply long-range homogeneous, following the theory exposed in section 2. This leads to an interaction window of a finite length $4L$, as $N \to \infty$, as shown in Fig. 9. Moreover, the stiffness is decreasing as $\chi/2^{|i|}$.

The equation of motion becomes:

$$\rho A \frac{\partial^2 u(x,t)}{\partial t^2} = EA \frac{\partial^2 u(x,t)}{\partial x^2} - \sum_{i=-N}^{0} \frac{\chi}{2^{|i|}} \left[u(x,t) - u\left(x + \frac{1-2^{|i|}}{2^{|i|-1}} L, t\right)\right] - \sum_{i=0}^{N} \frac{\chi}{2^{|i|}} \left[u(x,t) - u\left(x + \frac{2^{|i|}-1}{2^{|i|-1}} L, t\right)\right] \quad (13)$$

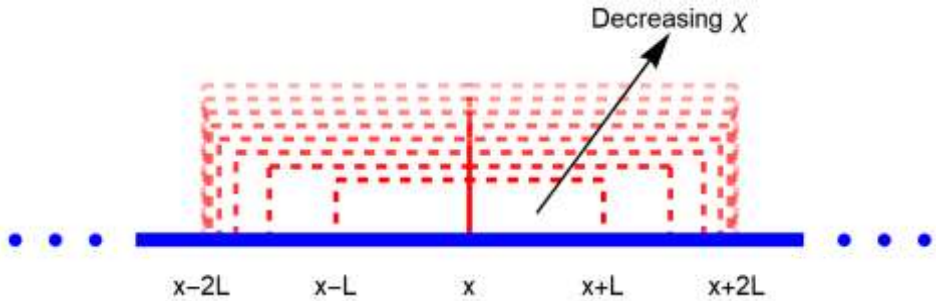


**Fig. 9:** Long-range homogenous waveguide with unequally spaced nonlocalities

The dispersion relation corresponding to Eq. (13) is:

$$K^2 - \Omega^2 + \mathrm{Z} \sum_{i=-N}^{0} \frac{\left[1 - e^{\frac{jK\left(1-2^{|i|}\right)}{2^{|i|-1}}}\right]}{2^{|i|}} + \mathrm{Z} \sum_{i=0}^{N} \frac{\left[1 - e^{\frac{jK\left(2^{|i|}-1\right)}{2^{|i|-1}}}\right]}{2^{|i|}} = 0 \quad (14)$$

and the group velocity curves associated to this case is represented in Fig. 10.

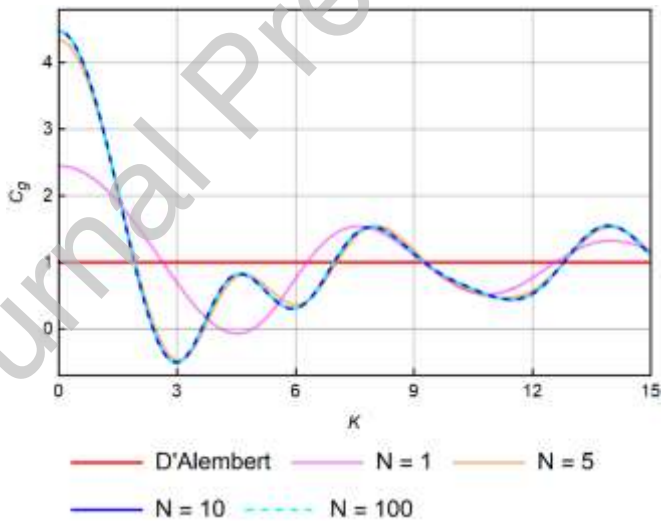


**Fig. 10:** Group velocity curves for the long-range homogenous waveguide with spacing $x_{i+1} - x_i = L/2^{|i|}$ and stiffness $\chi/2^{|i|}$. ($\mathrm{Z} = 10$)

Although an explicit formula may not be extracted, the figure demonstrates the convergence of the curves as $N \to \infty$. A critical value of Z for large $N$ is $\mathrm{Z}_{cr} \sim 4$, and below this threshold wave-stopping and negative group velocity can be observed.

Finally, the case of a continuous distribution of connectors remains with the definition of the kernel $G(x)$ as:

$$\rho A \frac{\partial^2 u(x,t)}{\partial t^2} = EA \frac{\partial^2 u(x,t)}{\partial x^2} - \chi \int_{-\infty}^{\infty} G(x-\zeta)\,[u(x) - u(\zeta)]d\zeta \tag{15}$$

The integral description of the long-range forces, replacing the summation of the previous examples, implies the existence of all possible interactions between the point $x$ and other points fallen within the window $G(x)$. Similar cases are available in the literature [16–19], investigating the plane-wave response of systems with confined regions of interaction.

Assuming $G(x) = [1 - cos\,(px)\,]/2^{|x|}$ with $p = \pi/L$, the above equation takes the form:

$$\rho A \frac{\partial^2 u(x,t)}{\partial t^2} = EA \frac{\partial^2 u(x,t)}{\partial x^2} - \frac{2p^2\chi}{(\ln 2)((\ln 2)^2+p^2)} u(x) + \chi\, \frac{[1-\cos(px)]}{2^{|x|}} * u(x) \tag{16}$$

where $*$ denotes the convolution operation. Since the area below the function $G(x)$ is finite, Eq. (16) describes a homogeneous-periodic waveguide with confined interaction region. Introducing the nondimensional parameters $\Omega = \omega\sqrt{\rho/E}/p$ , $K = k/p$ , $C = ln\, ln\, 2\, /p$ and $\mathrm{Z} = \chi/EAp^3$, the corresponding nondimensional dispersion relation is:

$$\Omega^2 = K^2 + \frac{2\mathrm{Z}}{C^3+C} + \frac{2\mathrm{Z}C(3K^2-1-C^2)}{(C^2+(K-1)^2)(C^2+(K+1)^2)(C^2+K^2)} \tag{17}$$

Both wave-stopping and negative group velocity phenomena are apparent in the response of this case as well, as shown in Fig. 11. Note that the negative group velocity band widens as Z increases.

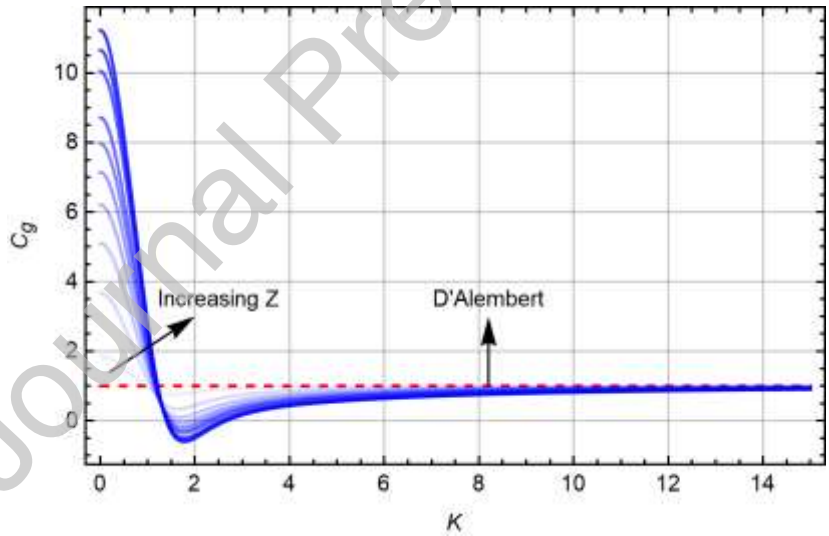


**Fig. 11:** Group velocity curves for the homogeneous-periodic waveguide with continuous connectivity

The examples presented in this section demonstrate the theoretical possibilities to control transmission of vibro-acoustic energy in waveguides using long-range interactions by means of adjusting frequencies, at which group velocity is not positive, to the prescribed ranges. These results path the way for innovative concepts of design of acoustic metamaterials. Recent advances in additive manufacturing suggest that the challenging task of implementing nonlocal links, which impose the long-range forces as described in this section, may be accomplished in a not too distant future.

However, at present, it is entirely feasible to introduce long-range forces between selected fixed stations in a waveguide.

## 4. Nonlocal non-homogenous periodic waveguides

Plane wave propagation of axial deformation in a uniform rod equipped with periodic long-range connectors, acting as spring-like links, is considered (see Fig. 12). This type of periodicity has been identified in section 2 as the long-range non-homogeneous one. In the graph-periodicity classification, this can be seen as a tree-periodic structure of period $L$ and leaf-periodic with same period, with only two leaves each tree ($N = 2$).

As first glance, it may be perceived as a yet another example of a waveguide composed of periodic mass-spring elements, which mimic nonlocal interactions, see, among many others, [29–31,35,39–43]. However, the distinctive feature of the periodic waveguide shown in Fig. 12 is the absence of inertial elements connected to the springs. Then, in contrast to all abovementioned references, periodic attachments do not introduce additional degrees of freedom as compared with a uniform continuous waveguide. On the other hand, instantaneous force transmission thoroughly substantiated in section 3 is considered here in a different setup, than in the previous sections. To the best of our knowledge, no detailed studies of the effects generated by the co-existence of conventional energy transmission in a periodic continuous waveguide and its instantaneous transfer by non-inertial long-range operators between fixed equally spaced stations in the same waveguide have been reported in the literature. This and subsequent sections of the paper fill in this gap.

The method of analysis used for this kind of systems is based on the Floquet theorem and is different with respect the direct method of double Fourier transform used for homogeneous periodicity.

Same notations as those in the previous sections are used for the mechanical and geometrical characteristics of the system. Note that, in this section, $L$ represents the length of non-deformed springs, which is the same as the length of the rod segments.

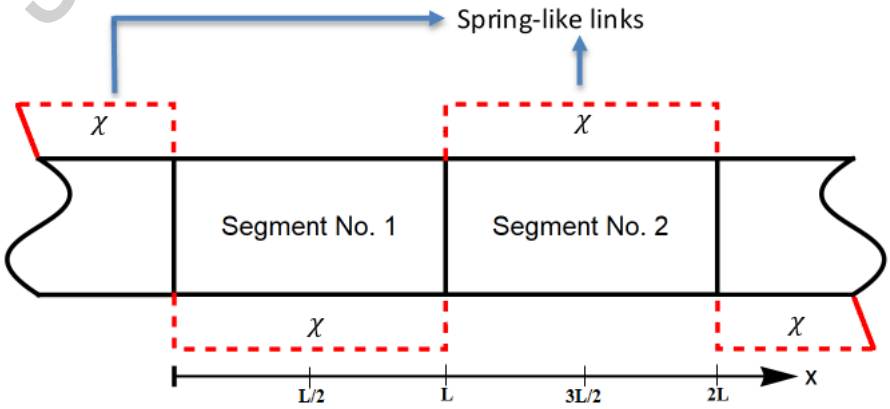


**Fig. 12:** A uniform rod with periodic nonlocalities

As already mentioned, the functionality of the spring elements in this structure differs from the classical periodic configurations, where springs are assembled in various configurations with discrete masses to compose a waveguide [39–43] or resonators attached to a unit-cell [29–31].

Although the equation of motion in Newtonian form for this structure is given in section 2, a variational principle is more practical for the identification of the interfacial and periodicity conditions. We apply Hamilton's principle $\delta H = 0$ for the action integral in the canonical form:

$$H = \int_{t_1}^{t_2} (T - U)\, dt \tag{18}$$

The total elastic energy $U$ stored in a rod (see Fig. 12) and its kinetic energy $T$ are given by:

$$U = \frac{1}{2}\left[\int_0^L EA\left(\frac{\partial u_1}{\partial x}\right)^2 dx + \int_L^{2L} EA\left(\frac{\partial u_2}{\partial x}\right)^2 dx\right] + \frac{1}{2}\chi[(u_1(L,t) - u_1(0,t))^2 + (u_2(2L,t) - u_2(L,t))^2] \tag{19a}$$

$$T = \frac{1}{2}\left[\int_0^L \rho A\left(\frac{\partial u_1}{\partial t}\right)^2 dx + \int_L^{2L} \rho A\left(\frac{\partial u_2}{\partial t}\right)^2 dx\right] \tag{19b}$$

where $u_1$ and $u_2$ are the axial displacements corresponding to segments number one and two, respectively.

The governing equation of motion for longitudinal waves for each segment, based on the Hamilton's principle, is:

$$\begin{cases} \frac{\partial^2 u_1(x,t)}{\partial t^2} = \frac{1}{c^2}\frac{\partial^2 u_1(x,t)}{\partial x^2}, \ x \in [0, L] \\ \frac{\partial^2 u_2(x,t)}{\partial t^2} = \frac{1}{c^2}\frac{\partial^2 u_2(x,t)}{\partial x^2}, \ x \in [L, 2L] \end{cases} \tag{20}$$

Here, $c^2 = E/\rho$ is the speed of the sound.

This textbook wave equation is an obvious simplification of Eq. (8) in absence of continuously distributed long-range forces. The effect of nonlocalities (or 'springs', as sketched in Fig. 12) within the framework defined by Eq. (19) is taken into account not in the governing differential equation as in previous section, but in the matching relations, extracted from stationarity conditions for the action integral (18), as:

$$u_1\rfloor_L - u_2\rfloor_L = 0 \tag{21a}$$

$$EA\frac{\partial u_1}{\partial x}\rfloor_L - EA\frac{\partial u_2}{\partial x}\rfloor_L + \chi[u_1(L,t) - u_1(0,t)] + \chi[u_2(L,t) - u_2(2L,t)] = 0 \tag{21b}$$

Now the periodicity conditions for a unit-cell should be formulated. As generally recognised, the choice of such a cell is not unique. However, once a symmetric periodicity cell is considered, positions of pass- and stopbands coincide with its eigenfrequencies for fixed-fixed and free-free boundary conditions [38]. Thus, we formulate periodicity conditions for a periodicity-cell 'chopped' from $x = L/2$ to $x = 3L/2$ in a waveguide (see Fig. 12):

$$u_1\rfloor_{L/2} - \Lambda\, u_2\rfloor_{3L/2} = 0 \tag{22a}$$

$$\frac{\partial u_1}{\partial x}\rfloor_{L/2} - \Lambda\, \frac{\partial u_2}{\partial x}\rfloor_{3L/2} = 0 \tag{22b}$$

where $\Lambda$ is a nondimensional parameter related to the canonical Bloch parameter $K_B$ as $\Lambda = e^{iK_B}$. This choice enables a more straightforward discussion of the results than by interpreting them in terms of $K_B$. Indeed, for $|\Lambda| = 1$, a wave/energy transmission is observed. In opposite, for any value such that $|\Lambda| \neq 1$, stopbands occur in the dynamic response of the structure and the energy transmission is terminated.

In order to reduce the number of involved parameters in this problem, the system of equations (21) and (22) is converted into the nondimensional form as:

$$\hat{u}_1\rfloor_1 - \hat{u}_2\rfloor_1 = 0 \tag{23a}$$

$$\frac{\partial \hat{u}_1}{\partial X}\rfloor_1 - \frac{\partial \hat{u}_2}{\partial X}\rfloor_1 + \mathrm{Z}\left[\hat{u}_1\rfloor_1 - \hat{u}_1\rfloor_0\right] + \mathrm{Z}\left[\hat{u}_2\rfloor_1 - \hat{u}_2\rfloor_2\right] = 0 \tag{23b}$$

$$\hat{u}_1\rfloor_{1/2} - \Lambda\, \hat{u}_2\rfloor_{3/2} = 0 \tag{23c}$$

$$\frac{\partial \hat{u}_1}{\partial X}\rfloor_{1/2} - \Lambda\, \frac{\partial \hat{u}_2}{\partial X}\rfloor_{3/2} = 0 \tag{23d}$$

where $X = x/L$ and $\hat{u}_i = u_i/L$ $(i = 1, 2)$ and the nondimensional stiffness is $\mathrm{Z} = \chi L/EA$. For each segment of the periodic rod, the displacement field $\hat{u}_j(X, t)$, the general solution of Eq. (20), has the canonical form:

$$\hat{u}_j(X, t) = \varphi_j e^{i\omega X - i\Omega t} + \psi_j e^{-i\omega X - i\Omega t} \tag{24}$$

Here, $\omega = \Omega L/c$. Substitution of this solution ansatz in the system of Eqs. (22) yields a system of four linear homogeneous algebraic equations with respect to the amplitudes of the right- and left-going waves in each segment. The condition of existence of its nontrivial solution is

$$\Lambda^2 + q(\omega)\Lambda + 1 = 0 \tag{25}$$

with

$$q(\omega) = \frac{-2\,[\omega cos\,(\omega)\ + \mathrm{Z}\,sin\,(\omega)\,]}{\omega +\ \mathrm{Z}sin\,(\omega)} \tag{26}$$

The discriminant function $(DF)$ of the quadratic equation (25) is given by:

$$DF = -\frac{\omega sin\,(\omega)\,(2\mathrm{Z}(1-cos\,(\omega)\,)+\ \omega sin\,(\omega)\,)}{(\omega + \mathrm{Z}sin\,(\omega)\,)^2} \tag{27}$$

If this function is positive, the roots of equation (25) are real-valued and the frequency $\omega$ falls into a stopband. If this function is negative, roots are complex conjugate and the frequency $\omega$ belongs to a pass band. This discriminant is a function of two nondimensional parameters, stiffness and frequency, and the areas marked in Fig. 13 in red are those of stopbands and the light brown areas correspond to the pass bands. The borders between these regions are

defined by the condition $DF = 0$. To meet this condition, three different solutions for Eq. (27) are available and clearly, the trivial solution, shown in yellow, is not of interest. The second set of solutions requires $sin(\omega)$ to be zero, yielding $\omega = n\pi$, with $n$ being a natural number, which are distinctly shown in the figure with black solid lines. Eventually, the blue curves are associated with the third solution $\mathrm{Z} = -\omega \cot(\omega/2)/2$. As a side note, we observe the hardly surprising similarity of the diagram in Fig. 13 to the canonical Ince-Strutt diagram, which describes properties of solutions of Mathieu equation and distinguishes stable and unstable ones.

The analysis of free vibrations of a unit-cell with free ends yields eigenfrequencies defined by the third solution and by the condition $cos(\omega) = 1$. The second solution $\omega = n\pi$ perfectly matches the eigenfrequencies of the same unit-cell with both ends fixed. Obviously, the set of eigenfrequencies $\omega = 2n\pi$ is shared by the unit-cells with fixed-fixed and free-free boundary conditions. Therefore, these frequencies define the gaps of the zero width [35].

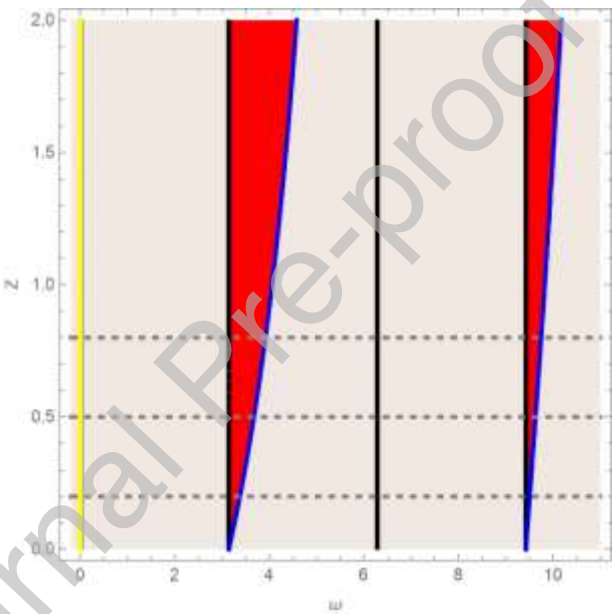


**Fig. 13:** Pass- and stopbands regions in the 'frequency-stiffness' plane: stopbands (red), passbands (light brown)

For consistency, frequency dependence of roots of the characteristic equation (25) is shown in Fig. 14 for three values of the stiffness parameter marked as horizontal lines in Fig. 12. As well-known from numerous papers, in passbands $|\Lambda| = 1$while the elliptic-like curves present purely real roots of the characteristic equation, $\Lambda_1\Lambda_2 = 1$, which define stopbands. The frequency, at which the stopband emerges, remains unchanged for different values of Z, as reported earlier by Fig. 13. The shape of standing wave at any boundary between pass- and stop-bands coincides with the eigenmode of vibration of a symmetric unit cell with either free-free or fixed-fixed boundary conditions. The eigenmodes of such a unit cell with free-free boundary conditions are such that the spring elements remain undeformed. Therefore, in this case neither eigenmodes nor eigenfrequencies are influenced by the magnitude of the stiffness parameter. Consequently, location of one border of any stopband is not dependent

on stiffness. An increase in stiffness makes stopband broader, as seen from both Fig. 13 and Fig. 14.

The phenomenon of cancellation of wave transmission has been demonstrated for the structures in the previous section; however, the current system provides a frequency band for achieving wave-stopping while the configurations are only capable of producing individual frequencies at which the phenomenon occurs.

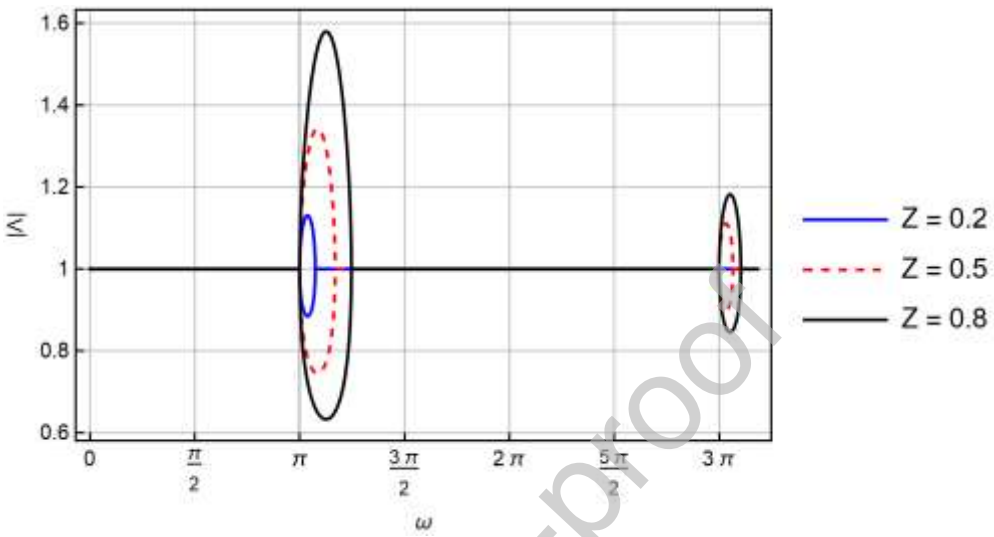


**Fig. 14:** Band structure for uniform waveguide with nonlocalities

Inspection of Eq. (27) suggests that $DF$ becomes singular when its denominator vanishes, producing:

$$Z = -\frac{\omega}{sin\,(\omega)} \tag{28}$$

This implies that one root of Eq. (25) tends to infinity and the other tends to zero. Thus, an infinitely large attenuation may be attained at a set of excitation frequencies for a given value of Z, a much desirable effect for vibro-isolation purposes. Note that this effect is unique to this specific kind of periodicity since it is induced as a result of periodic distribution of springs along the host structure. In the absence of these springs, the denominator of $DF$ simply collapses into $\omega$, and no similar effect emerges.

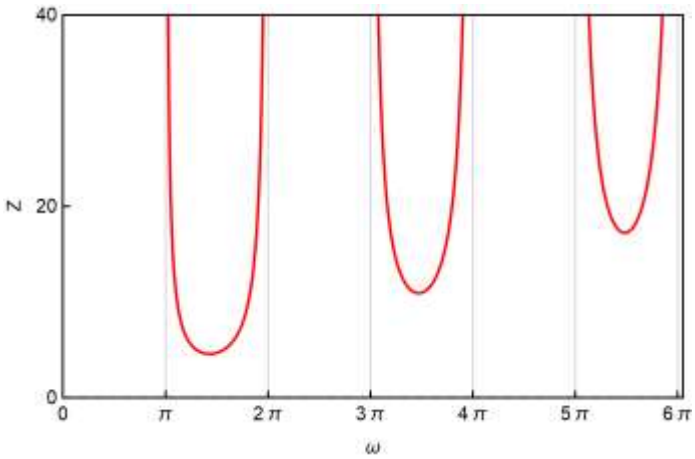

**Fig. 15:** Critical stiffness as a function of frequency

Fig. 15 shows the plot of Z yielded by Eq. (28), provided over a wide range of nondimensional stiffness. The infinite attenuation effect appears within regularly separated bandwidths. At lower frequencies, this 'complete', or 'ideal' attenuation may be obtained by deploying springs of relatively small stiffness, while this effect is more difficult to reach when the frequency increases, requiring higher spring stiffness. The minimum stiffness, which delivers infinite attenuation, is easily found by equating the first derivative of denominator of Eq. (25) to zero giving $tan(\omega_0) = \omega_0$. The first root is $\omega_0 = 4.721$ with the corresponding nondimensional stiffness $\mathrm{Z} = 4.721$. This point is brought up again in section 7, where the working mechanism of such configuration is investigated from an energy transfer point of view.

On balance, it is concluded that disruption of the energy transfer may be achieved using the instantaneous long-range forces between a priori selected fixed stations in a waveguide. Unlike the case considered in the previous section, the underlying physical mechanism employed here is the Bragg's destructive interference of waves, the 'trademark' of periodic waveguides.

## 5. Negative stiffness and low frequency stopbands

The desirable influence of stationed nonlocalities on the stopbands in terms of broadening stop bands and stronger attenuation wherein, especially at low frequencies, has been demonstrated in the previous section. However, the principle demand to pull the first stopband to the lowest possible frequencies has not been met neither using impedance mismatch [35] nor using the long-range interactions. Hence, an alternative view at the physics of the system is requested to accomplish this very highly demanding task. So far, the analysis has been limited to the physically meaningful positive values of the stiffness for the springs. Now the stiffness Z in Eq. (27) is allowed to attain negative values. Given that the rod segment and the springs can be considered as parallel springs, the analysis of the discriminant function is conducted over a particular stiffness range ($-1 \leq \mathrm{Z} \leq 0.2$) in Fig. 16 in order to assure the lack of occurrence of instability in the system. The figure shows the possibility of pulling the stopbands to low frequencies given a proper negative value for stiffness. Additionally, the inspection of Bloch parameter $K_B$ in this case suggest no particular abnormality with respect to the systems characterized by positive values of Z. Note that some contributions in the context of acoustics metamaterials [44–46] demonstrated the instability within certain thresholds while considering negative effective stiffness for their corresponding systems though such effect have not been recognised in the present study.

Although the negative values of stiffness are not compatible with conventional springs, devices exhibiting such a behaviour are very well-known and broadly used in vibration control, with an electro-magnetic system being an obvious example. Another possibility is an active control system, in which piezo elements are used to generate forces proportional to the instant difference in displacements of control points and acting in the requested direction.

Note that technicalities of practical implementation of this concept (and review of numerous publications on devices featuring negative stiffness) are not dwelled here. We just demonstrate the effect, which can be obtained by these means for the system we deal with.

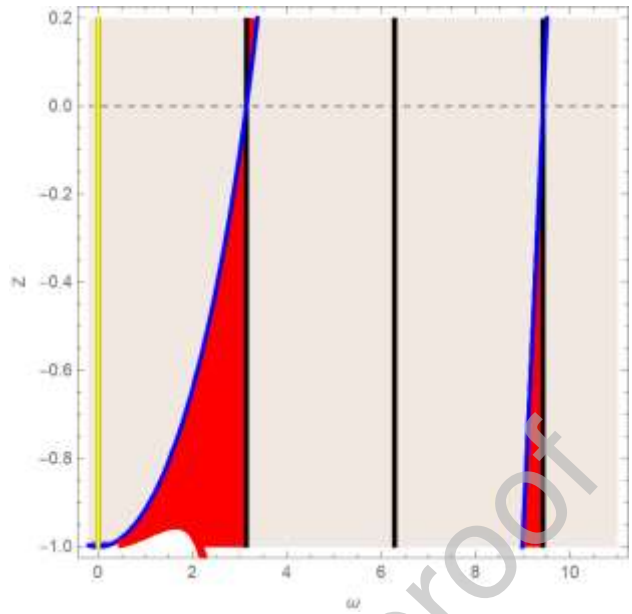


**Fig. 16:** Pass- and stopbands regions in the 'frequency-negative stiffness' plane: stopbands (red), passbands (light brown)

To conclude this section, we highlight the main similarity and the main differences between performances of an infinite periodic waveguide shown in Fig.12 and a conventional periodic waveguide, which features impedance mismatch between its constituents. Positions of the 'seed' frequencies, at which stop bands emerge as soon as an arbitrarily small impedance mismatch or a non-local operator is introduced, are the same - provided, of course, that the constituents of periodicity cells are of the same length. However, an infinitely large attenuation at the discrete set of frequencies, feasible due to non-locality (see Eq. (28) and Fig.15), cannot be produced by any realistic impedance mismatch. The second important difference is that the negative stiffness, unlike the conventional impedance mismatch, is capable to pull the stopband to an arbitrarily low frequency range.

## 6. Analysis of insertion losses

So far, our analysis has been confined to solution of problems in free wave propagation for nonlocal homogeneous and nonhomogeneous periodic waveguides. Further insights into their behaviour come from solutions of the forcing problem. Its standard formulation is associated with calculations of Insertion Losses (IL).

The insertion loss in dB is given by [47]:

$$IL = 10\log_{10} E_0/E_s \tag{29}$$

Here, $E_0$ is the energy flux (EF) in a semi-infinite uniform D'Alembert waveguide (i.e., with the springs removed) and $E_s$ denotes the EF in the same semi-infinite waveguide equipped

with an insert (i.e., with the non-local operators) in the same excitation conditions, as illustrated in Fig. 17. The EF averaged over a period of motion for a dilatation time-harmonic wave in a one-dimensional waveguide is [48]:

$$E(x) = -\frac{1}{2} Re[N_x(x)\underline{V}(x)] \tag{30}$$

where $N_x(x)$ and $\underline{V}(x)$ are the axial force and the conjugate of the axial velocity, respectively.

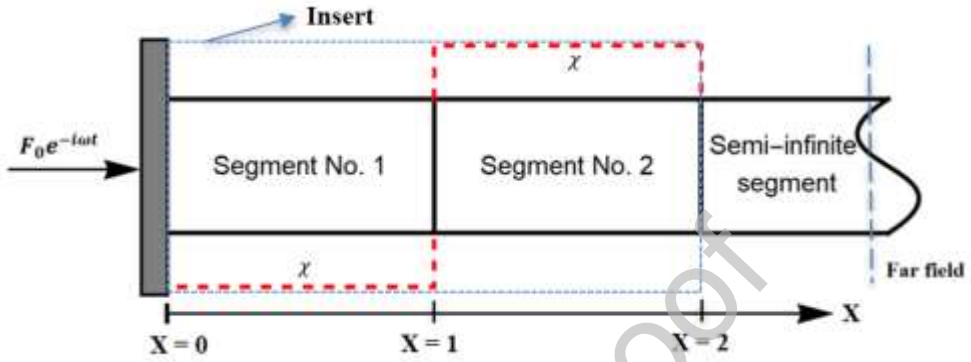


**Fig. 17:** Semi-infinite rod with the insert

Let us first consider a semi-infinite uniform waveguide with two long-range operators as shown in Fig. 17. Then the semi-infinite segment obeys Sommerfeld radiation condition and supports outgoing travelling wave, while pairs of direct and reflected waves are generated in segments 1 and 2. The amplitudes of these five waves are determined by using the following conditions:

$$\hat{F} - \frac{\partial \hat{u}_1}{\partial X}\rfloor_0 + \mathrm{Z}[\hat{u}_1\rfloor_0 - \hat{u}_1\rfloor_1] = 0 \tag{31a}$$

$$\hat{u}_1\rfloor_1 - \hat{u}_2\rfloor_1 = 0 \tag{31b}$$

$$\frac{\partial \hat{u}_1}{\partial X}\rfloor_1 - \frac{\partial \hat{u}_2}{\partial X}\rfloor_1 + \mathrm{Z}[\hat{u}_1\rfloor_1 - \hat{u}_1\rfloor_0] + \mathrm{Z}[\hat{u}_2\rfloor_1 - \hat{u}_2\rfloor_2] = 0 \tag{31c}$$

$$\hat{u}_2\rfloor_2 - \hat{u}_3\rfloor_2 = 0 \tag{31d}$$

$$\frac{\partial \hat{u}_2}{\partial X}\rfloor_2 - \frac{\partial \hat{u}_3}{\partial X}\rfloor_2 + \mathrm{Z}[\hat{u}_2\rfloor_2 - \hat{u}_2\rfloor_1] = 0 \tag{31e}$$

Here, $\hat{F} = F/EA$. Solving the above system fully characterizes the wave motion in the system. As already shown by various studies, insertion loss $IL$ at the frequencies inside the stopbands is significantly higher with respect to those within pass bands. In fact, insertion loss is a mean to distinguish passbands from the stopbands, and its increase corresponds to the magnitude of $\Lambda$ within stopbands.

Fig. 18 compares the insertion loss as in Eq. (29) for three different cases, i.e. two, three and four unit-cells. Based on the figure, the peaks are located around stopbands already predicted by the Floquet analysis. Indeed, the loss at stopband frequencies is notably large, which virtually verifies the performance of the infinite structure presented beforehand (see Fig. 14).

Furthermore, it is apparent how the higher the number of unit-cells, the larger the amplitude of peaks around the stopband frequencies. It is worth mentioning that for a limited number of unit-cells, the bandwidth of the peaks does not precisely determine the bandwidth of the associated stopbands. Eventually, the plot suggests the existence of points at which the insertion loss becomes null for all the curves. These points have been defined as shared points. Furthermore, each curve presents other points of null insertion loss, but those are strictly related to the number of the unit-cells in the insert. The discussion that follows is devoted to the physical interpretation of all these points of zero insertion loss.

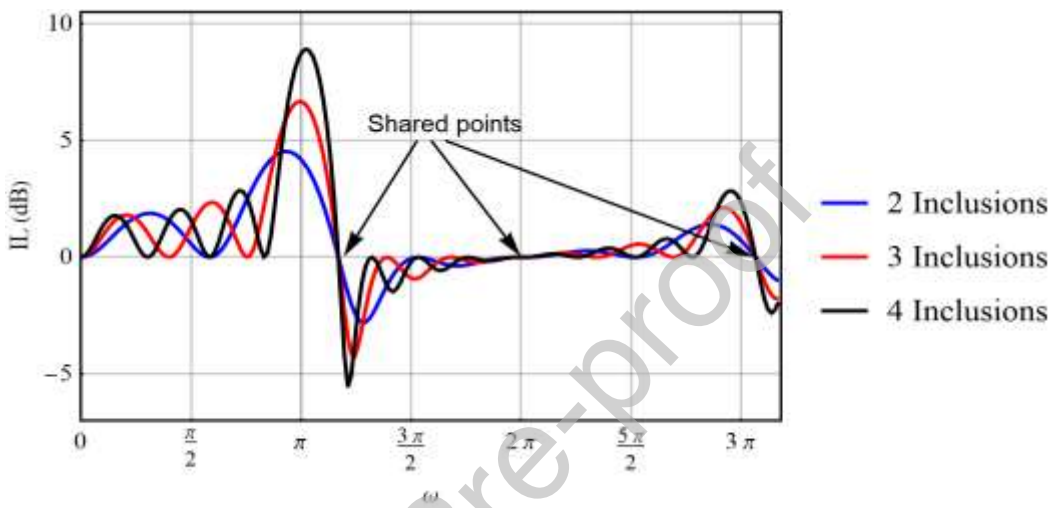


**Fig. 18**: Insertion loss for a semi-infinite uniform waveguide with nonlocalities ($Z = 0.5$)

In the above figure, regardless of the number of unit-cells in the insert, there are shared points at which the insert is fully transparent, i.e. $IL = 0$. In Ref. [38], it is shown how the eigenfrequencies associated to the free-free unit-cell of a periodic structure are related to borders of stopbands. The eigenfrequency equations of the associated stopband are $\cos(\omega) = 1$ and $Z + \omega \cot(\omega/2)/2 = 0$. Since the shared points occur exactly at these eigenfrequencies, it is clear how there is a one-to-one correspondence between shared points and borders of these stopbands. In addition to the shared points, there are other points on each curve, where $IL = 0$. These zeros correspond to eigenfrequencies of the corresponding insert with both ends free. To further explain the correspondence between shared points and stopbands, Fig. 19 reports the single case of three unit-cells.

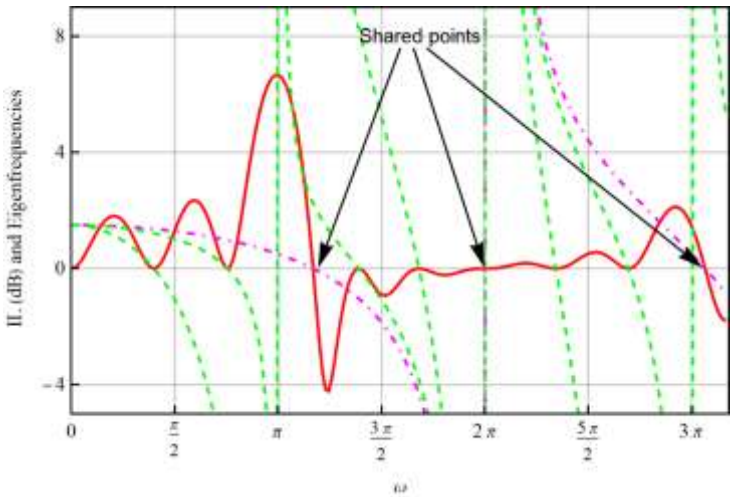


**Fig. 19:** Red curve: insertion losses for the three/component periodic structure ($Z = 0.5$), Magenta lines: Eigenfrequency equation of a unit-cell with free ends, Green curves: Unique eigenfrequency equations associated with the free-free insert with three unit-cells.

Fig. 19 presents the case of a semi-infinite structure with an insert composed of three unit-cells to highlight the above comments. The global behaviour is partially determined by the collective characteristics of the insert, and by the intrinsic properties of the single unit-cell (see Fig. 17). Indeed, the figure shows, more than the trend of the insertion loss $IL$ (red solid curve), the eigenfrequencies of the insert, green dashed curves, and the eigenfrequencies of the unit-cell, magenta dot-dashed curves, all with respect to the nondimensional frequency. The behaviour of the insert is expressed by two separate equations, namely $Z + 2\omega\cot(\omega) - \omega/\sin(\omega) = 0$ and $Z + 2\omega\cot(\omega)/3 + \omega/3\sin(\omega) = 0$: the green curves and; since the insert changes according to the number of unit-cells, it carries the information regarding the zeros related to the specific structure. These zeros belong to the pass band frequencies, since they fall outside the major peaks, as shown in Fig. 18. It is worth mentioning that the zeros corresponding to the magenta curve are the shared points, identical to those exhibited in Fig. 18, due to the presence of the unit-cell in each insert.

## 7. Analysis of Energy Flux Partition

As pointed out in section 4, the distinctive feature of a nonlocal nonhomogeneous periodic waveguide is the co-existence of the energy transport in its conventional 'continuous' path and the instantaneous energy transfer by non-inertial long-range operators. As seen from equation (30a), the driving time-harmonic force $\hat{F}$ at $x = 0$ is balanced by two components: a force in the segment 1 and a nonlocal force in the spring. This is illustrated in Fig. 17 and now in Fig. 20 as a textbook setup 'springs in parallel' for a single insert in a semi-infinite waveguide. However, since we consider an open system with the energy leakage to the far field, the division of the external force to two components entails similar energy partition, as sketched in Fig. 20.

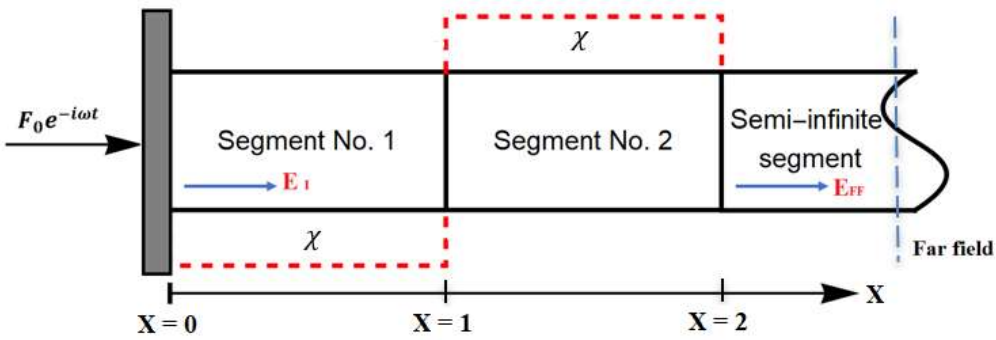


**Fig. 20:** The energy transmission partition in the semi-infinite uniform rod with nonlocalities

The force acquired by the segment 1 at $x = 0$ generates the conventional energy transmission across the segments by a travelling wave at the finite speed $c$ in the amount $E_I$ (see Fig. 20). Since the material losses are excluded, this energy is conveyed in full to the end of insert. This is the action of a primary source, well known in acoustics. The non-inertial springs transmit their part of a driving force instantaneously to the right end of the first cell, so do all the other springs till the end of last cell. Then the instantaneous "spring-borne" force acts at the right end of the insert as a secondary source. Naturally, the interaction between these sources may be either constructive or destructive. Such a secondary source cannot exist in the conventional periodic compound rods, and it induces appreciable changes in the energy flux. Indeed, while in conventional periodic structures with no material losses energy flux does not depended upon the distance $x$, here it experiences a jump at the interface between the insert and the semi-infinite segment, see Fig. 20. In Ref. [40], the similar effect is called 'tunnelling power flow', which, however, is customarily understood in a different sense [49]. To assess the interaction between the primary and the secondary source, the energy flux $E_I$ injected into the rod at $x = 0$, where the external force is applied, and the energy flux $E_{FF}$ (i.e. in the far field) in the semi-infinite segment are compared:

$$EFP = 10 \log_{10} E_I / E_{FF} \tag{32}$$

where EFP, in dB, stands for energy flux partition. It is straightforward, using the mathematical induction method, to prove that, in contrast to insertion losses, this characteristic is independent upon the number of unit-cells in the periodic insert and is defined by the elementary formula:

$$EFP = 10 \log_{10} \frac{\omega}{\omega + \mathrm{Z} sin(\omega)} \tag{33}$$

This function is plotted in Fig. 21 for $\mathrm{Z} = 0.5$. As long as $\omega < \pi$, the constructive interference takes place as the secondary source cooperates with the primary source and adds to the energy flowing through the rod from $x = 0$. Indeed, negative values of EFP are produced whenever $E_I < E_{FF}$. At the frequency $\omega = \pi$, $EFP = 0$, implying no energy injection produced by the force transmitted via springs and a constant energy flux along the whole structure. Recalling Eq. (30), this condition occurs, when the spring force is shifted by $\pi/2$ with respect to the complex conjugate of the velocity. When $\omega$ becomes larger than $\pi$, the inequality sign swaps: $E_I > E_{FF}$, see Fig. 21. Thus, positive values of $EFP$ imply that the

secondary source opposes the energy transmission to the far field, i.e. destructive interference takes place. Transitions between constructive and destructive interference occur frequency-wise every $\pi$. At each 'switching frequency' $\omega = n\pi$ $(n = 2, 3, 4, \dots, N)$, with $N$ being a positive integer, the force imposed by the end spring does not contribute in the energy flux.

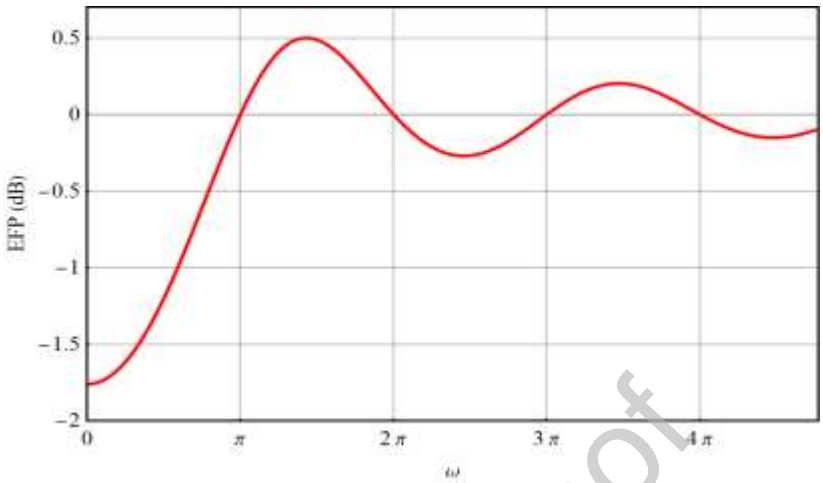


**Fig. 21**: Energy flow partition (Z = 0.5)

Note how Eq. (33) recalls Eq. (26), where EFP turns to infinity at the set of frequencies defined by Eq. (26), given a large enough value of Z. The chosen value of the stiffness, namely

$Z = 0.5$ does not correspond to any of the crossings of the curves shown in Fig. 15, and thereby no infinite attenuation occurs. However, a different choice of Z (larger values) would imply no energy can be transferred to the far field at these frequencies.

For clarity, it should be emphasised that quantity Energy Flux Partition introduced and analysed in this section is completely different from the insertion losses dealt with in section 6, despite that both involve the energy flux in a far field for a waveguide with an insert. In IL, this energy flux is referred to the energy flux in a uniform waveguide, so that IL strongly depend upon the number of periodicity cells. In EFP the reference is the amount of energy which travels with the conventional speed c in the rod from the point $x = 0$, where the external force is applied, to the end on the periodic insert. This quantity does not depend upon the number of periodicity cells in an insert.

## 8. Concluding remarks

The wave propagation in a conventional rod (canonical D'Alembert waveguide) integrated with nonlocalities, which provide long-range interactions, is investigated. The combination of the concepts of nonlocality and periodicity leads to identify a rather general notion named graph-periodicity. As a corollary, two different kinds of long-range periodicity emerge: homogeneous, and non-homogenous, or genuine periodicity. First, the wave propagation in four homogeneous waveguides is analysed using nonlocal interactions. This type of periodicity implies the tree-periodicity disappears, in that any arbitrary point in a waveguide is linked to a set of other points located within an open or confined interaction region. The

possibility of stopping the energy flow at individual frequencies, provided that the nonlocalities are sufficiently stiff, is demonstrated. Furthermore, it is revealed that the backward energy transmission is met within certain frequency bands with their boundaries being the wave-stopping frequencies. Next, the canonical Floquet theory is used to obtain explicit formulas defining location of pass- and stopbands for the genuine periodic waveguide with non-homogeneous long-range interactions between fixed stations along its length. Stopbands are generated without the conventional impedance mismatch. The set of frequencies, at which the band gaps emerge, is independent upon the stiffness of the external elastic links. This set coincides with the eigenfrequencies of a unit periodicity cell. An excellent agreement is observed between the results extracted from preceding analysis and those from computing insertion losses in the semi-infinite uniform rod equipped with a periodic insert having a variable number of unit periodicity cells. The physical explanation of frequency-dependence of insertion losses is based on the adopted model of instantaneous long-range interactions, which implies the generation of a secondary source at the end of the periodic insert. Finally, the model predicts the ultra-low-frequency band gaps, which may even emerge from zero, for a specific negative value of stiffness. In this situation, the long-range interaction may be thought of as a result of active control. As for the future work, besides the obvious experimental demonstration, investigating the transient response by solving the Cauchy problem for the forcing of rod with limited number of unit-cells and non-reflecting boundary could be of the interest. The overall results concluded throughout the paper suggests that the implementation of nonlocalities into a conventional waveguide can cause disruption in the energy transmission across the domain.

**Credit author statement**

**A. S. Rezaei:** Methodology, Software, Formal analysis, Writing-Original Draft, Writing-Review & Editing, Visualization.

**A. Carcaterra**: Conceptualization, Methodology, Writing- Review & Editing, Supervision.

**S. V. Sorokin**: Conceptualization, Methodology, Formal analysis, Writing- Review & Editing, Supervision.

***A. Hvatov:*** Formal analysis.

**F. Mezzani**: Writing-Original Draft, Writing-Review & Editing.

**Declaration of Conflicting Interests**

The author(s) declared no potential conflicts of interest with respect to the research, authorship, and/or publication of this article.

**References**

[1] L. Brillouin, Wave propagation in periodic structures electric filters and crystal lattices., Dover Publications, [New York], 1953.

[2] A.C. Eringen, Plane waves in nonlocal micropolar elasticity, Int. J. Eng. Sci. 22 (1984) 1113–1121.

[3] A.C. Eringen, Linear theory of nonlocal elasticity and dispersion of plane waves, Int. J. Eng. Sci. 10 (1972) 425–435.

[4] A.C. Eringen, Linear Theory of Micropolar Elasticity, J. Math. Mech. 15 (1966) 909–923.

[5] Eringen, A.Cemal, Edelen, D.G.B., On nonlocal elasticity, Int. J. Eng. Sci. 10 (1972) 233–248.

[6] S.A. Silling, Reformulation of elasticity theory for discontinuities and long-range forces, J. Mech. Phys. Solids. 48 (2000) 175–209.

[7] A. Madeo, G. Barbagallo, M.V. D'Agostino, L. Placidi, P. Neff, First evidence of non-locality in real band-gap metamaterials: Determining parameters in the relaxed micromorphic model, Proc. R. Soc. A Math. Phys. Eng. Sci. 472 (2016).

[8] V.E. Tarasov, Lattice with long-range interaction of power-law type for fractional non-local elasticity, Int. J. Solids Struct. 51 (2014) 2900–2907.

[9] V.E. Tarasov, Continuous limit of discrete systems with long-range interaction, J. Phys. A. Math. Gen. 39 (2006) 14895.

[10] V.E. Tarasov, G.M. Zaslavsky, Fractional dynamics of systems with long-range interaction, Commun. Nonlinear Sci. Numer. Simul. 11 (2006) 885–898.

[11] M. Di Paola, G. Failla, M. Zingales, Physically-Based Approach to the Mechanics of Strong Non-Local Linear Elasticity Theory, J. Elast. 97 (2009) 103–130.

[12] I.A. Kunin, Elastic Media with Microstructure I, Springer Berlin Heidelberg, Berlin, Heidelberg, 1982.

[13] M. Di Paola, A. Pirrotta, M. Zingales, Mechanically-based approach to non-local elasticity: Variational principles, Int. J. Solids Struct. 47 (2010) 539–548.

[14] A. Carpinteri, P. Cornetti, A. Sapora, A fractional calculus approach to nonlocal elasticity, Eur. Phys. J. Spec. Top. 193 (2011) 193–204.

[15] M. Zingales, Wave propagation in 1D elastic solids in presence of long-range central interactions, J. Sound Vib. 330 (2011) 3973–3989.

[16] A. Carcaterra, F. Coppo, F. Mezzani, S. Pensalfini, Metamaterials: Wave propagation control, in: Proc. ISMA 2016 - Int. Conf. Noise Vib. Eng. USD2016 - Int. Conf. Uncertain. Struct. Dyn., 2016.

[17] F. Mezzani, F. Coppo, S. Pensalfini, N. Roveri, A. Carcaterra, Twin-waves propagation phenomena in magnetically-coupled structures, in: Procedia Eng., Elsevier Ltd, 2017: pp. 711–716.

[18] F. Coppo, A.S. Rezaei, F. Mezzani, S. Pensalfini, A. Carcaterra, Waves path in an elastic membrane with selective nonlocality, in: Proc. ISMA 2018 - Int. Conf. Noise Vib. Eng. USD 2018 - Int. Conf. Uncertain. Struct. Dyn., 2018.

[19] A. Carcaterra, F. Coppo, F. Mezzani, S. Pensalfini, Long-Range Retarded Elastic Metamaterials: Wave-Stopping, Negative, and Hypersonic or Superluminal Group

Velocity, Phys. Rev. Appl. 11 (2019) 014041.

[20] F. Mezzani, A.S. Rezaei, A. Carcaterra, Wave Propagation Phenomena in Nonlinear Elastic Metamaterials, in: New Trends Nonlinear Dyn., Springer International Publishing, 2020: pp. 31–40.

[21] A. Rezaei, F. Mezzani, A. Carcaterra, Wave propagation with long-range forces and mistuning effects, Proc. Inst. Mech. Eng. Part C J. Mech. Eng. Sci. (2021) 095440622198974.

[22] D.J. Mead, Wave propagation in continuous periodic structures: Research contributions from Southampton, 1964-1995, J. Sound Vib. 190 (1996) 495–524.

[23] Applications of ATILA FEM Software to Smart Materials - 1st Edition, (n.d.). https://www.elsevier.com/books/applications-of-atila-fem-software-to-smart-materials/uchino/978-0-85709-065-2 (accessed November 17, 2020).

[24] M.M. Sigalas, E.N. Economou, Elastic waves in plates with periodically placed inclusions, J. Appl. Phys. 75 (1994).

[25] I.E. Psarobas, N. Stefanou, A. Modinos, Scattering of elastic waves by periodic arrays of spherical bodies, Phys. Rev. B - Condens. Matter Mater. Phys. 62 (2000) 278–291.

[26] J.C. Hsu, T.T. Wu, Lamb waves in binary locally resonant phononic plates with two-dimensional lattices, Appl. Phys. Lett. 90 (2007).

[27] M. Sigalas, E.N. Economou, Band structure of elastic waves in two dimensional systems, Solid State Commun. 86 (1993) 141–143.

[28] L. Fok, M. Ambati, X. Zhang, Acoustic metamaterials, MRS Bull. 33 (2008) 931–934.

[29] H. Sun, X. Du, P.F. Pai, Theory of metamaterial beams for broadband vibration absorption, J. Intell. Mater. Syst. Struct. 21 (2010) 1085–1101.

[30] R. Zhu, X.N. Liu, G.K. Hu, C.T. Sun, G.L. Huang, A chiral elastic metamaterial beam for broadband vibration suppression, J. Sound Vib. 333 (2014).

[31] C. Yang, L. Cheng, Suppression of bending waves in a beam using resonators with different separation lengths, J. Acoust. Soc. Am. 139 (2016).

[32] Y. Cheng, J.Y. Xu, X.J. Liu, One-dimensional structured ultrasonic metamaterials with simultaneously negative dynamic density and modulus, Phys. Rev. B - Condens. Matter Mater. Phys. 77 (2008) 045134.

[33] H.H. Huang, C.T. Sun, G.L. Huang, On the negative effective mass density in acoustic metamaterials, Int. J. Eng. Sci. 47 (2009).

[34] Y. Shanshan, Z. Xiaoming, H. Gengkai, Experimental study on negative effective mass in a 1D mass-spring system, New J. Phys. 10 (2008).

[35] R.B. Nielsen, S. V. Sorokin, Periodicity effects of axial waves in elastic compound rods, J. Sound Vib. 353 (2015) 135–149.

[36] S. V. Sorokin, On propagation of plane symmetric waves in a periodically corrugated straight elastic layer, J. Sound Vib. 349 (2015) 348–360.

[37] A.S. Rezaei, S. V. Sorokin, F. Mezzani, A. Carcaterra, Band structure of elastic bodies with periodic nonlocalities, in: EURODYN, 2020: pp. 2457–2463.

[38] A. Hvatov, S. Sorokin, Free vibrations of finite periodic structures in pass- and stop-bands of the counterpart infinite waveguides, J. Sound Vib. 347 (2015) 200–217.

[39] G. Hu, L. Tang, R. Das, Internally coupled metamaterial beam for simultaneous vibration suppression and low frequency energy harvesting, J. Appl. Phys. 123 (2018) 055107.

[40] L. Quan, A. Alù, Hyperbolic Sound Propagation over Nonlocal Acoustic Metasurfaces, Phys. Rev. Lett. 123 (2019) 244303.

[41] E. Ghavanloo, S.A. Fazelzadeh, Wave propagation in one-dimensional infinite acoustic metamaterials with long-range interactions, Acta Mech. 230 (2019) 4453–4461.

[42] H. Zhu, S. Patnaika, T.F. Walsh, B.H. Jared, F. Semperlotti, Nonlocal elastic metasurfaces: Enabling broadband wave control via intentional nonlocality, Proc. Natl. Acad. Sci. U. S. A. 117 (2020) 26099–26108.

[43] P.P. Pratapa, P. Suryanarayana, G.H. Paulino, Bloch wave framework for structures with nonlocal interactions: Application to the design of origami acoustic metamaterials, J. Mech. Phys. Solids. 118 (2018) 115–132.

[44] G. Hu, L. Tang, J. Xu, C. Lan, R. Das, Metamaterial with Local Resonators Coupled by Negative Stiffness Springs for Enhanced Vibration Suppression, J. Appl. Mech. Trans. ASME. 86 (2019).

[45] G. Hu, J. Xu, L. Tang, C. Lan, R. Das, Tunable metamaterial beam using negative capacitor for local resonators coupling, J. Intell. Mater. Syst. Struct. 31 (2020) 389–407.

[46] W.J. Drugan, Wave propagation in elastic and damped structures with stabilized negative-stiffness components, J. Mech. Phys. Solids. 106 (2017) 34–45.

[47] C. L. Morfey, The Dictionary of Acoustics , Academic Press , 2000.

[48] L. Cremer, M. Heckl, B.A.T. Petersson, Structure-borne sound: Structural vibrations and sound radiation at audio frequencies, Springer Berlin Heidelberg, 2005.

[49] J.B. Keller, Uniform solutions for scattering by a potential barrier and bound states of a potential well, Am. J. Phys. 54 (1986) 546–550.